Lab on a Chip

PAPER

Syringe-pump-induced fluctuation in all-aqueous microfluidic system implications for flow rate accuracy†

Cite this: *Lab Chip*, 2014, **14**, 744

Zida Li,[a] Sze Yi Mak,[a] Alban Sauret[b] and Ho Cheung Shum*[ac]

Received 16th October 2013,
Accepted 19th November 2013

DOI: 10.1039/c3lc51176f

www.rsc.org/loc

We report a new method to display the minute fluctuations induced by syringe pumps on microfluidic flows by using a liquid–liquid system with an ultralow interfacial tension. We demonstrate that the stepper motor inside the pump is a source of fluctuations in microfluidic flows by comparing the frequencies of the ripples observed at the interface to that of the pulsation of the stepper motor. We also quantify the fluctuations induced at different flow rates, using syringes of different diameters, and using different syringe pumps with different advancing distances per step. Our work provides a way to predict the frequency of the fluctuation that the driving syringe pump induces on a microfluidic system and suggests that syringe pumps can be a source of fluctuations in microfluidic flows, thus contributing to the polydispersity of the resulting droplets.

1. Introduction

In the last decade, microfluidic technology has been shown to be a powerful tool to generate emulsions,[1] which are of great importance in various fields including food industry, cosmetics, drug delivery, and oil extraction.[2–6] Many properties of emulsions are related to their sizes, which therefore need to be controlled. Monodispersity is a major advantage of microfluidic emulsification when compared to other methods, such as mechanical agitation, and has inspired intense research efforts to apply microfluidic droplets. In classical microfluidic methods involving syringe pumps, the generation of droplets is done in a passive way through a Rayleigh–Plateau instability which breaks a jet into droplets; size is expected to be uniformly distributed across droplets.[2,7–13] The exquisite control brought by microfluidic methods enables the generation of droplets with size polydispersity of typically less than 5% and usually between 1% and 3%, as reported in previous experimental studies.[13–16] However, the exact source of the polydispersity remains unexplored. The precision of the measurement techniques, such as image analysis, probably accounts for part of the polydispersity. Variability in the operating flow conditions may also play a role, but detailed studies have been limited by the inability to detect any sort of fluctuations in microfluidic flows.

Microfluidic flows used to generate emulsions can be characterized by parameters such as the viscosity of the two phases, their densities, the channel diameter and the interfacial tension.[2] These quantities are unlikely to fluctuate in a controlled environment; for instance, the temperature does not fluctuate sufficiently to contribute to the size polydispersity observed. Among the parameters, the flow rates of the two phases represent the most likely candidate source of fluctuation. Until now, flow rates delivered by syringe pumps are believed to be highly precise despite the lack of measurement approaches to precisely quantify and visualize the flow rate delivered by syringe pumps in microfluidic systems.[17] By tracking the interface in a two-phase flow, fluctuations in the flow rates can potentially be detected. Indeed, as the flow rate fluctuates, the diameter of the inner jet varies,[18] leading to a deformation of the interface and formation of ripples.[19] Classical oil–water systems used in microfluidics have an interfacial tension around 20 mN m^{-1} (ref. 20) and exhibit no visible fluctuation of the jet of one phase in the other. Because of this relatively large surface tension, the minute fluctuations are typically not visible, as the interfacial tension effects tend to minimize the interfacial area and smoothen the interface. In addition, the amplitude of the fluctuation that syringe pumps induce is expected to be small;[21,22] therefore, the fluctuation can hardly be visualized at the interface. To do so, a fluid system characterized by an ultra-low interfacial tension is needed. Recently, many studies have focused on aqueous two-phase systems, which consist of two immiscible aqueous solutions of incompatible macromolecules such

[a] *Department of Mechanical Engineering, The University of Hong Kong, Pokfulam Road, Hong Kong, China. E-mail: ashum@hku.hk*
[b] *Department of Mechanical and Aerospace Engineering, Princeton University, Princeton, New Jersey 08544, USA*
[c] *HKU-Shenzhen Institute of Research and Innovation (HKU-SIRI), Shenzhen, China*

† Electronic supplementary information (ESI) available: (1) Methods of measurement of frequency of ripples and (2) same ripples observed with another syringe pump of same model. See DOI: 10.1039/c3lc51176f

as polymers. The nature of the two phases leads to an ultra-low interfacial tension, typically 10^{-5} to 10^{-4} N m^{-1}, much smaller compared to a classical oil-in-water system where the interfacial tension is more than 100 times larger.[23,24] The use of all-aqueous systems decreases the damping due to capillary effects of the initial perturbation and allows the visualization of previously undetectable fluctuations in the fluidic environment.

In this paper, we report a method to display the minute fluctuations that syringe pumps induce with an aqueous two-phase system. We consider two co-flowing streams and observe the ripples generated at the interface (see Fig. 1(a)). Because of the ultra-low interfacial tension, the interface is highly sensitive and easily deformed by perturbations.[25] By comparing the frequencies of the resultant ripples and of the pulsations in the flow rate, we confirm that the stepper motor inside the syringe pump is a source of the fluctuations. Visual examination of the ripples provides a simple way to estimate the upper bound of the amplitude of these fluctuations. Our work provides an approach to characterize pulsations in syringe pumps and suggests the possibility for manipulating multiphase flow by minute vibrations.

2. Experimental methods

The device used in our experiments is a common glass capillary microfluidic device, which consists mainly of a cylindrical and a square glass capillary,[26–29] as illustrated in Fig. 2(a). The cylindrical glass microcapillary, with an outer diameter of 1.0 mm, is tapered to the desired diameter, around 50 μm,

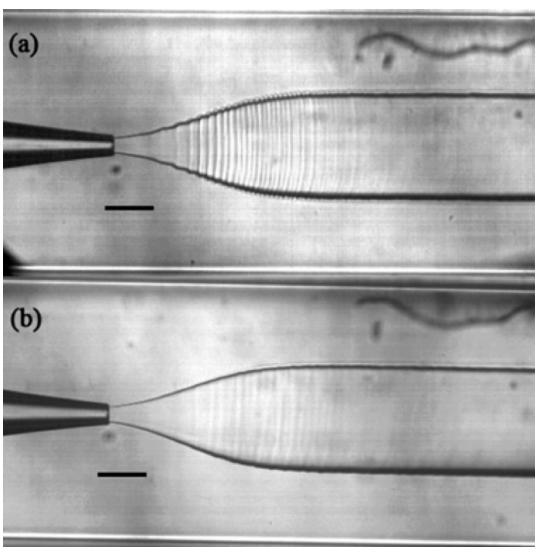

Fig. 1 Optical microscope image of an inner jet surrounded by a continuous phase. The inner phase is a 15 wt% tripotassium phosphate (K_3PO_4) solution, and the outer phase is a 17 wt% polyethylene glycol (PEG, MW = 8000) solution. (a)The fluids are driven by syringe pumps (LSP01-2A), and the flow rates of the inner and outer phases are Q_{in} = 4 mL h^{-1} and Q_{out} = 7 mL h^{-1}, respectively. (b) The fluids are driven by pressure-driven pumps. The estimated flow rates are Q_{in} = 3.6 mL h^{-1} and Q_{out} = 4.9 mL h^{-1}. Scale bars are 200 μm.

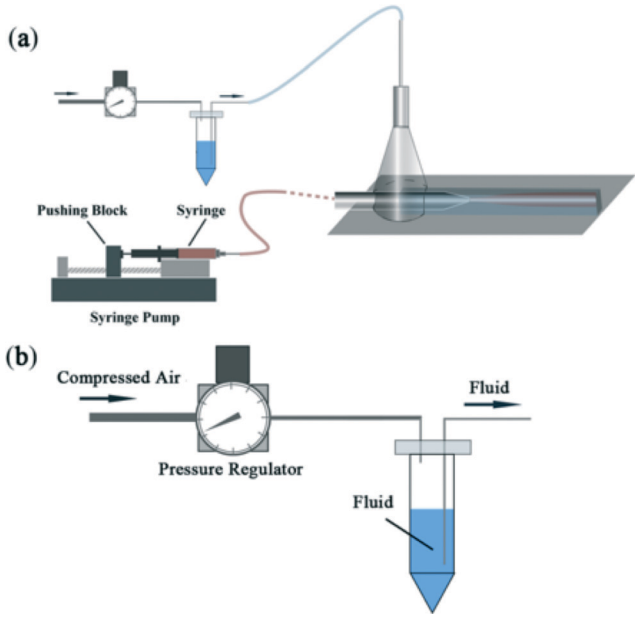

Fig. 2 Schematic of the experimental setup. (a) A pressure-driven pump dispenses the outer phase into the square outer capillary through a needle, and a syringe pump drives the inner phase into the cylindrical inner capillary. (b) Pressure-driven pump setup. Pressurized air flows through a pressure regulator and flows out at constant pressure. Then the air fills a gas tight reservoir, which in turn pushes the fluid out.

and then co-axially aligned within the square capillary, whose inner dimension is 1.05 mm. The outer phase of a polyethylene glycol (PEG, 17% wt, MW = 8000) solution flows in the square capillary, while the inner phase of a tripotassium phosphate (K_3PO_4, 15% wt) solution flows in the cylindrical inner capillary. The interfacial tension of the two phases is estimated to be around 0.03 mN m^{-1}.[30] The two fluids meet at the tip of the inner capillary and form a jet (see Fig. 1(a–b)). We observe the ripples at the interface of the jet using an inverted optical microscope (XD-101, Jiangnan, Inc.) equipped with a high speed camera (MotionPro X4, Redlake, Inc.) at typically 4000 frames per second. After recording a high-speed movie of the ripples, three methods are used to measure the frequency depending on the quality of the images and displacement of the ripples (see ESI,† S1). We ensured that these three methods lead to similar results when applied to the same experiment. In the first method, we process the images to identify the interface, observe the oscillations of the interface at a certain location, and obtain the frequency spectrum by applying a Discrete Fourier Transform. This process usually gives a spectrum with the single largest peak corresponding to the dominant frequency component. We then fit the spectrum to a Gaussian curve and obtain the mean frequency associated with the ripples and the corresponding variance. In the second method, we observe the periodic changes in the apparent grayscale intensity on the interface due to the differing lensing effects from the oscillating jet diameter. We pick the grayscale value at a point in each frame and apply the same transform and fitting method as mentioned above to obtain the mean frequency and variance. In the third method,

we count the ripples manually and then calculate the mean frequency and variance.

Unless otherwise mentioned, the inner phase is contained in glass syringes (SGE 10 mL gas tight syringe, internal diameter 14.57 mm) and injected to the device using syringe pumps (longer pump model LSP01-2A, advancing distance per step, s = 0.03125 μm), while the outer phase is dispensed using a pressure-driven pump. The stepper motor inside a syringe pump supplies the driving force for the fluid to be injected in the device. For each step of the motor, the pushing block (see Fig. 2(a)) moves forward over a given distance, leading to a pulse, which can be a source of disturbance in the flow rate of the syringe pump. We obtain the disturbance frequency associated with the stepper motor, f_{pulse}, by calculating the number of steps of the pushing block per second. The corresponding frequency of pulsation is thus given by

$$f_{\text{pulse}} = \frac{4Q}{\pi D^2 s} \quad (1)$$

where s represents the advancing distance per step of the pushing block, Q is the fluid flow rate and D is the internal diameter of the syringe which depends on the model considered. To vary this last parameter, we also use another two syringes with different internal diameters (SGE 5 mL and Hamilton 25 mL gas tight syringe, with internal diameters D = 10.30 mm and D = 23.03 mm, respectively). To consider the influence of the advancing distance per step, s, we also performed experiments with another model of syringe pump characterized by a different advancing parameter (Cole Parmer Model EW-4900-45, advancing distance per step, s = 0.165 μm). In this study, we highlight the influence of a syringe pump on the fluctuation of the flow rate. For comparison, we also performed some experiments using a pressure-driven pump, as illustrated in Fig. 2(b). Pressurized air flows through a pressure regulator and flows out at constant pressure. The air fills a gas-tight reservoir, which in turn pushes the fluid through a piece of tubing into the device. This system is expected to present less fluctuations than the syringe-pump system though the pressure regulator may also introduce some tiny fluctuations.

3. Results and discussions

To detect the minute fluctuations of the inner fluid flow rate Q_{in}, we co-flow an aqueous two-phase system characterized by an ultra-low interfacial tension[23] and monitor the interface. Indeed, when both fluids are injected using syringe pumps, regular and periodic ripples are observed, as reported in Fig. 1(a). We then replace the two syringe pumps with pressure-driven pumps. With this method, the amplitude of the fluctuation is significantly reduced and the associated frequency becomes irregular, as shown in Fig. 1(b). Note that some ripples are still observed, likely due to the spring loading force from the pressure regulator and the surrounding environment, such as tiny vibrations of the benchtop. This result confirms that the periodic ripples are largely caused by the fluctuations generated during liquid dispensing by the syringe pump and also confirms the sensitive nature of the interface in the aqueous two-phase system.[14] To ensure that the fluctuations do not originate from a faulty syringe pump, we repeat the experiments using different syringe pumps of the same model, and similar ripples are observed (see Fig. S5 in ESI†); this suggests that the ripples are generic to the systems with syringe pumps. To identify the source of ripples, we repeat the experiments and systematically vary the flow rates of both the inner and the continuous phases. The frequency of the ripples, f_{ripples}, only depends on the flow rate of the inner phase, Q_{in} (see Fig. 3). Indeed, since the cross sectional area occupied by the continuous phase close to the nozzle is about 500 times larger than that occupied by the inner phase, for the flow rates considered here, the mean velocity of the continuous phase is two orders of magnitude smaller than that of the inner phase. Therefore, the wavelength of the fluctuations induced by the outer phase is too small to be observed. The frequency of the ripples, f_{ripples}, is identical to the frequency of the pulsations of the syringe pump that drives the inner phase, $f_{\text{pulse}} = 4Q/(\pi D^2 s)$, as calculated with relation (1) (see Fig. 3). Therefore, these observations suggest that the ripples visible at the interface between the two immiscible phases are induced by the pulsation of the stepper motor in the syringe pump and that each advancing step causes one pulse.

Based on the above hypothesis, the frequency of the pulsations should vary according to the speed at which the relevant components in the stepper motor move. This speed depends on various parameters, such as the flow rates, the internal diameter of the syringe, and the advancing distance per step (which depends on the design of the syringe pump and is provided by the manufacturer). If the ripples are caused by the pulsations of the syringe pump, their frequency is expected to show a unique dependence

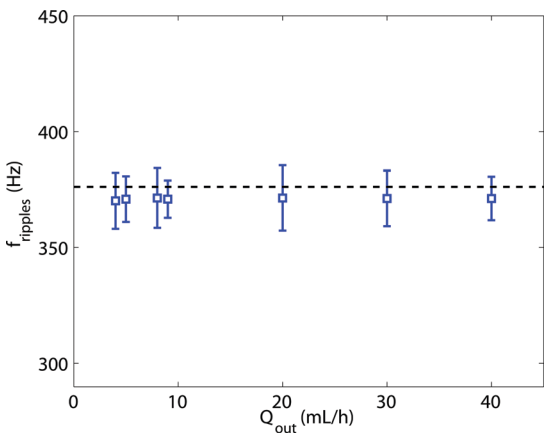

Fig. 3 Frequency of the ripples f_{ripples} as a function of the flow rate of the outer phase Q_{out} while the inner phase is injected at a constant flow rate Q_{in} = 7 mL h^{-1} using a 10 mL syringe driven by an LSP01-2A syringe pump. The squares with error bars are the measured frequency of ripples, and the continuous line is the frequency of fluctuation induced by the syringe pump that drives the inner fluid, estimated with relation (1).

on these parameters. For a given combination of a syringe pump and a syringe, an increase in the flow rate is achieved by a proportionate increase in the advancing speed of the stepper motor. Therefore, the frequency of the ripples is expected to increase linearly with an increasing target flow rate, as indicated by relation (1). In addition, if we consider a syringe with a different diameter, the advancing speed of the stepper motor should change accordingly to maintain the same fluid flow rate as predicted by relation (1), leading to a different pulsation frequency. Thus the ripple frequency, $f_{ripples}$, should scale with the diameter of the syringe as D^2 for constant flow rates and step size of the motor. This suggests that a proper rescaling of the frequency by D^2 should lead to a collapse of the data for a given model of syringe pump. The linear dependence is indeed observed; the data for the different syringe pumps can indeed be collapsed onto a single curve, as shown by the comparison of the experimentally observed and the predicted frequencies of the ripples as a function of the target flow rate in Fig. 4. Experimentally, we have obtained the relationship between the ripple frequencies and driving flow rates for three different syringes with different internal diameters (10.30 mm, 14.57 mm and 23.03 mm). The experimental results are in excellent agreement with the prediction based on the above relationship, as shown in Fig. 4.

Our results suggest that the ripple frequency can be precisely predicted if the dispensing conditions and the configurations of the syringe pump are known. To confirm this, we repeat the experiments using a syringe pump of a different brand with different specifications, and we calculate the predicted ripple frequencies for different flow rates and syringes of different internal diameters, using the new advancing distance per step of the motor. Indeed, the observed ripple frequencies are precisely predicted (see Fig. 5). These results confirm our hypothesis that each observed ripple at the all-aqueous interface with ultralow interfacial tension is triggered by an advancing step of the stepper motor. To the best of our knowledge, this is the first systematic and direct visualization and confirmation of the fluctuations in flow rates induced by syringe pumps. Our approach can serve as a test for checking the advancing step size of syringe pumps against their specifications.

Another important parameter to quantify is the amplitude of the fluctuation of the flow rate, but it is more difficult to predict. Consider a jet of radius r_j in an axisymmetric co-flow capillary of radius R. We estimate the amplitude by approximating that, to first order, the dimensionless radius of the jet, $r = r_j/R$, is the same as in an axisymmetric capillary of equivalent diameter $D = 2L/\sqrt{\pi} = 1185\,\mu m$ (where $L = 1.05$ mm is the thickness of the square capillary). Then, in this axisymmetric capillary of radius R, r is related to the ratio of the inner Q_{in} and outer Q_{out} flow rates, as well as the viscosity of the inner η_{in} and outer η_{out} phases through the relation:[18]

$$\frac{Q_{in}}{Q_{out}} = \frac{2r^2}{1-r^2} + \frac{\eta_{out}}{\eta_{in}}\frac{r^4}{(1-r^2)^2} \quad (2)$$

The geometry of the problem described in the above experiments is more complicated to model due to its deviation from the axisymmetric case, since the outer capillary has a square cross-section rather than a circular one. However, for simplicity, we will use the previous equation as an approximation to estimate the amplitude of the flow rate fluctuations. We denote δQ_{in} and δr as the fluctuations of the flow rates and the jet radius, respectively; therefore:

$$Q_{in} = Q_{in,0} + \delta Q_{in} \text{ and } r = r_0 + \delta r \quad (3)$$

With small fluctuations, *i.e.* $\delta Q_{in}/Q_{in,0} \ll 1$ and $\delta r/r_0 \ll 1$, relation (2) leads, to first order in δr and after simplification, to

$$\frac{\delta Q_{in}}{Q_{out}} = \frac{4\,\delta r}{1-r_0^2}\left(r_0 + \frac{r_0^3}{1-r_0^2}\right)\left(1 + \frac{\eta_{out}}{\eta_{in}}\frac{r_0^2}{1-r_0^2}\right) \quad (4)$$

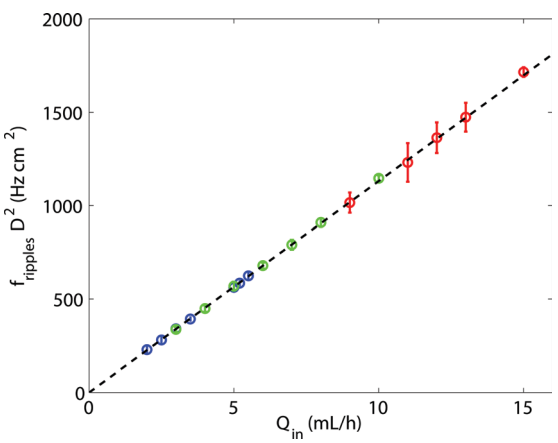

Fig. 4 Frequency of the ripples as a function of the flow rate of the inner phase Q_{in} for different sizes of syringes, driven by an LSP01-2A syringe pump. Data points with error bars denote the measured frequencies of ripples for different syringe diameters: blue (SGE 5 mL), green (SGE 10 mL), and red (Hamilton 25 mL). The black dashed-dotted line is the analytical prediction given by relation (1).

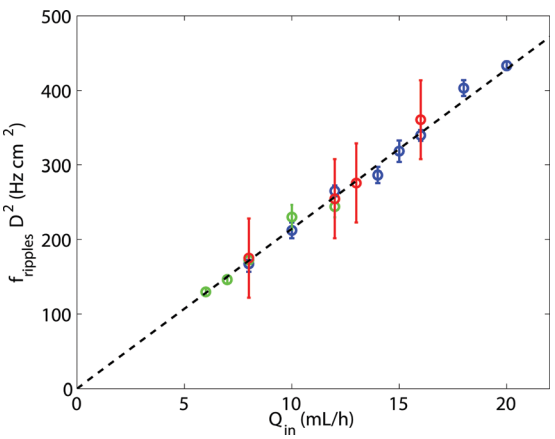

Fig. 5 Same as Fig. 4 but with different syringe pumps, Cole Parmer EW-74900-45, whose advancing distance per step is 0.165 μm.

To highlight the effects of stepper motors in syringe pumps on the fluctuations in flow rates dispensed, we pick the syringe pump with the largest amplitude of fluctuations, probably due to aging of the machine parts and prolonged usage (Fig. 1). We extract the experimentally observed average diameter of the jet, d_{jet} as well as the amplitude of the fluctuation of the jet radius, δr, and obtain d_{jet} = 435 μm, δd = 2 and δr = 13 μm in a capillary of equivalent diameter D = 1185 μm. The viscosity values of the inner and outer fluids are η_{in} = 1.37 mPa s and η_{out} = 13.0 mPa s, respectively. Using these values and expression (4), we obtain an estimate of the inner flow rate fluctuation for the parameters used in Fig. 1(a), $\delta Q_{in}/Q_{in}$ ~ 0.09. From this simple model, the fluctuations in flow rate due to the syringe pump are estimated to be around 9%. Despite the fact that our capillary is not axisymmetric and relation (1) or (2) may not be totally adapted, we have been able to provide a first estimate of the amplitude of perturbation. The uncertainty obtained is an upper bound since the estimation is performed using data from a driving syringe pump that is known to provide pronounced fluctuations in flow rates. In a normal microfluidic operation, the observed fluctuations are likely much smaller on the order of 1–2%. Our experimental results thus provide a simple way to estimate both the frequency and amplitude of fluctuations in flow rates caused by the syringe pump used. To estimate the polydispersity of the resulting emulsion generated with such a syringe pump, we apply a scaling law previously derived for the diameter of droplets formed by the breakup of a widening jet.[27] The drop diameter is shown to be related to the inner fluid flow rate Q_{in} and the velocity of the outer phase u_{out}, through the relation

$$d_{drop} \sim \left(\frac{Q_{in}}{Q_{out}}\right)^{1/2} \quad (5)$$

The polydispersity of the emulsion droplets is therefore estimated to be:

$$\frac{\delta d_{drop}}{d_{drop}} \sim \frac{1}{2}\frac{\delta Q_{in}}{Q_{in}} + \frac{1}{2}\frac{\delta u_{out}}{u_{out}} \quad (6)$$

For the system considered here, a syringe pump dispenses the inner fluid, and a pressure-driven pump dispenses the outer fluid. Therefore, the uncertainty in the outer fluid flow rates is much smaller than that for the inner fluid flow rate. Based on this approach, the polydispersity is estimated to be $\delta d_{drop}/d_{drop}$ ~ $\delta Q_{in}/2Q_{in}$ ~ 4.5%. Despite the simplifying assumptions, our approach suggests that the perturbation in the flow rates induced by the syringe pump can lead to variations in the size of the droplets which are of the same order as the measurements reported in the literature.[13–15] Using this approach, 1–2% fluctuations in the flow rates delivered by the corresponding syringe pumps will result in a polydispersity in droplet size of about 0.5–1%. The variability in the values of polydispersity reported may be due to the difference in the performance of different syringe pumps.

4. Conclusions

In this article, we report the first visualization of fluctuations induced by a syringe-pump in a liquid–liquid system with ultralow interfacial tension by observing the generated ripples on the interface. These ripples, which are normally hidden in systems with a much higher interfacial tension, are visible due to the passive nature of the all-aqueous interface with significantly lower tension. We quantitatively characterize the ripples against different flow rates, syringe diameters, and step sizes of the syringe pumps and also provide a first estimate of the amplitude of the fluctuations. These results confirm our hypothesis that each ripple is generated by one moving step of the stepper motor. Our work provides an approach to characterize syringe pumps, based on microfluidic flows, to unprecedented precision and inspires a new way to detect minute fluctuations in flow rates. We also show that the small variation of the flow rate induced by syringe pumps potentially plays a role in contributing to the polydispersity of emulsions.[13–16] Furthermore, the sensitivity of the interface reported here suggests the possibility to manipulate fluid dynamics in passive interfaces through minute vibrations including sound waves. By varying the flow rate in a controlled manner, it is foreseeable to form interfacial ripples with tunable frequency and amplitude, as we have deduced in this work. This provides an opportunity to correlate the deformation of the interface to the variation of the flow rates.

Acknowledgements

This research was supported by the Early Career Scheme (HKU 707712P) from the Research Grants Council of Hong Kong, the Basic Research Program-General Program (JC201105190878A) from the Science and Technology Innovation Commission of Shenzhen Municipality, the Young Scholars Program (NSFC51206138/E0605) from the National Natural Science Foundation of China, as well as the Small Project Funding (201109176165) and the University Development Fund (UDF) on A Soft Lithography System for Fabrication of Microfluidic Devices from the University of Hong Kong.

References

1 G. M. Whitesides, *Nature*, 2006, **442**, 368–373.
2 H. A. Stone, A. D. Stroock and A. Ajdari, *Annu. Rev. Fluid Mech.*, 2004, **36**, 381–411.
3 T. M. Squires and S. R. Quake, *Rev. Mod. Phys.*, 2005, **77**, 977.
4 O. A. Basaran, *AIChE J.*, 2002, **48**, 1842–1848.
5 W. J. Duncanson, T. Lin, A. R. Abate, S. Seiffert, R. K. Shah and D. A. Weitz, *Lab Chip*, 2012, **12**, 2135–2145.
6 T. Franke, L. Schmid, D. A. Weitz and A. Wixforth, *Lab Chip*, 2009, **9**, 2831–2385.

7 J. C. McDonald and G. M. Whitesides, *Acc. Chem. Res.*, 2002, **35**, 491–499.
8 S. K. Sia and G. M. Whitesides, *Electrophoresis*, 2003, **24**, 3563–3576.
9 D. Erickson and D. Li, *Anal. Chim. Acta*, 2004, **507**, 1–26.
10 Q. Xu, M. Hashimoto, T. T. Dang, T. Hoare, D. S. Kohane, G. M. Whitesides, R. Langer and D. G. Anderson, *Small*, 2009, **5**, 1575–1581.
11 F. Zendejas, U. Srinivasan, W. Holtz, J. D. Keasling and R. T. Howe, *13th Int. Conf. on Solid-State Sensors, Actuators and Microsystems*, 2005, 1473–1476.
12 J. Xu, S. Li, J. Tan, Y. Wang and G. Luo, *Langmuir*, 2006, **22**, 7943–7946.
13 P. Garstecki, H. A. Stone and G. M. Whitesides, *Phys. Rev. Lett.*, 2005, **94**, 164501.
14 D. Link, S. Anna, D. Weitz and H. Stone, *Phys. Rev. Lett.*, 2004, **92**, 054503.
15 S. Xu, Z. Nie, M. Seo, P. Lewis, E. Kumacheva, H. A. Stone, P. Garstecki, D. B. Weibel, I. Gitlin and G. M. Whitesides, *Angew. Chem.*, 2005, **117**, 734–738.
16 A. S. Utada, E. Lorenceau, D. R. Link, P. D. Kaplan, H. A. Stone and D. A. Weitz, *Science*, 2005, **308**, 537–541.
17 T. Ward, M. Faivre, M. Abkarian and H. A. Stone, *Electrophoresis*, 2005, **26**, 3716–3724.
18 A. Sauret and H. Shum, *Int. J. Nonlinear Sci. Numer. Simul.*, 2012, **13**, 351–362.
19 A. Sauret, C. Spandagos and H. C. Shum, *Lab Chip*, 2012, **12**, 3380–3386.
20 C. N. Baroud, F. Gallaire and R. Dangla, *Lab Chip*, 2010, **10**, 2032–2045.
21 B. S. Mohammed, D. A. Fields, B. Mittendorfer, A. R. Coggan and S. Klein, *Metab., Clin. Exp.*, 2004, **53**, 875–878.
22 M. L. Cordero, F. Gallaire and C. N. Baroud, *Phys. Fluids*, 2011, **23**, 094111.
23 S. Hardt and T. Hahn, *Lab Chip*, 2012, **12**, 434–442.
24 Y. Song, A. Sauret and H. C. Shum, *Biomicrofluidics*, 2013, DOI: 10.1063/1.4827916.
25 H. C. Shum, A. Sauret, A. Fernandez-Nieves, H. A. Stone and D. A. Weitz, *Phys. Fluids*, 2010, **22**, 082002.
26 R. K. Shah, H. C. Shum, A. C. Rowat, D. Lee, J. J. Agresti, A. S. Utada, L.-Y. Chu, J.-W. Kim, A. Fernandez-Nieves and C. J. Martinez, *Mater. Today*, 2008, **11**, 18–27.
27 A. S. Utada, A. Fernandez-Nieves, H. A. Stone and D. A. Weitz, *Phys. Rev. Lett.*, 2007, **99**, 094502.
28 A. Sauret and H. Shum, *Appl. Phys. Lett.*, 2012, **100**, 145106.
29 H. Shum, J. Varnell and D. Weitz, *Biomicrofluidics*, 2012, **6**, 012808.
30 C.-W. Kim and C. Rha, *Phys. Chem. Liq.*, 2000, **38**, 25–34.